Induced dipole effect in strong-field photodetachment of atomic negative ions

V. E. Chernov,[1] I. Yu. Kiyan,[2,*] H. Helm,[2] and B. A. Zon[1,†]
[1]*Voronezh State University, University Sq. 1, 394006 Voronezh, Russia*
[2]*Albert-Ludwigs-Universität, D-79104 Freiburg, Germany*
(Received 28 September 2004; published 21 March 2005)

The process of strong-field photodetachment of an atomic negative ion is considered with a simple analytical account for the ac dipole moment induced in the atomic core by the external laser field. The method is based on a Keldysh-like saddle-point theory, modified by using dipole-spherical angular wave functions in the initial state of the outer electron. The field-induced dipole results in an increase of the detachment rate and essential modifications in its angular dependence. These modifications are interpreted as destruction of the quantum interference originated from the coherent superposition of the two saddle-point contributions to the transition amplitude.

DOI: 10.1103/PhysRevA.71.033410 PACS number(s): 42.50.Hz, 32.80.Gc

I. INTRODUCTION

In the last two decades, multiphoton photodetachment of atomic negative ions has been a subject of intense experimental studies [1–6]. The experimental results were interpreted using various theoretical models: simplified Hartree-Fock (HF) calculations [7], multiconfiguration HF (MCHF) calculations [8] with the final electron state described by close-coupling scattering [9] or by the L^2 method [10], quasistationary quasienergy state (QQES) approach [11] recently generalized for nonzero angular momentum [12], single-electron perturbation calculations [13–16], many-body perturbation theory (random-phase approximation with exchange [17] and Dyson equation [18]), different versions of *B*-spline [19], *R*-matrix [20–24], and multichannel quantum defect (MQDT) methods [25–27] (for more references on theoretical treatment of multiphoton detachment of negative ions see the reviewing articles [14,28–30]).

In the strong-field regime, when the number of absorbed photons is large, most of the above-mentioned theoretical methods become difficult to implement and cannot provide an adequate description of photodetachment. Meanwhile, recent experiments on H^- [5] and F^- [6] ions show that the strong-field photodetachment is well described by a simple Keldysh-like theory [31,32]. However, a weakness of such a theory is its essential one-electron nature. At the same time, the many-electron effects are well known to affect significantly both the electronic structure [33] and the low-field photodetachment [29] of negative ions. The one-electron methods can be corrected by using model potentials which account for many-body effects. One significant effect is the dipole moment induced by the outer electron in the atomic core due to its static polarizability α. At large distances r of the outer electron the corresponding model polarization potential has the asymptotic form (atomic units are used throughout)

$$V^{\mathrm{pol}}(r) \sim -\frac{\alpha}{2r^4}. \tag{1}$$

Potential (1) is known to significantly influence the electron affinity [34]; it was used in descriptions of few-photon [24] and dc-field [35] detachment of negative ions. However, the electron-induced polarization potential (1) does not describe dynamical many-body effects which arise in an external ac field due to the core polarization by the field. This field-induced dipole moment of the atomic core involves its dynamical (i.e., frequency-dependent) polarizability $\alpha(\omega)$ instead of its static value.

The effects of the ac field-induced dipole moment in atomic photoprocesses have been studied for a long time. Such effects in bound-bound transitions (oscillator strengths) were studied in Ref. [36]. The bound-free transitions (few-photon detachment) were considered using perturbation theory in Refs. [13–15,28]. The free-free transitions affected by the field-induced dipole are known as polarization bremsstrahlung and were reviewed in Ref. [37]. Reference [38] contains a review of all three types of transitions.

Our aim in the present work is to elaborate on an analytical method which accounts for the ac field-induced dipole in strong-field photodetachment of negative ions. The numerical calculations are performed for Rb^- and Cs^- anions because of their large atomic polarizabilities. In our consideration we follow the Keldysh-like theory formulated by Gribakin and Kuchiev [32], which we modify by using an earlier nonperturbative description [39,40] of dipole effects with the help of dipole-spherical functions.

The alkali-metal anions are chosen for two purposes. First, the large polarizabilities of the corresponding atoms should result in larger magnitudes of the considered effect. Second, one-electron approximation is satisfactory for a qualitative analysis of these systems due to a comparatively large distance between the valent electron and the atomic core. To achieve more precise results, several powerful computation methods can be applied [41,42]. These methods are developed to solve numerically the time-dependent Schrödinger equation for a "real" atomic system with two or more active electrons in a strong laser field. While their power in computation is highly suitable for a detailed comparison of experiment and theory [43], their drawback is that the underlying physics is lost behind numerics. Instead, the

*Electronic address: igor.kiyan@physik.uni-freiburg.de
†Electronic address: zon@niif.vsu.ru

 ©2005 The American Physical Society

analytical method used in this work allows us to identify the effect of quantum interference, which is present in the process of photodetachment by a linearly polarized field. We show below how this effect vanishes due to the angular electron correlations.

II. GENERAL FORMALISM

An outer electron is removed from a negative ion by interaction with the linearly polarized laser field

$$\boldsymbol{F}(t) = \boldsymbol{F}\cos\omega t, \quad V_F(t) = -\boldsymbol{r}\cdot\boldsymbol{F}(t). \tag{2}$$

The differential detachment rate has the form [32]

$$dw = \sum_n dw_n = 2\pi\sum_n |A_{pn}|^2 \delta\left(\frac{\boldsymbol{p}^2}{2} + U_p - E_0 - n\omega\right)\frac{d^3p}{(2\pi)^3}, \tag{3}$$

where $E_0 = -\varkappa^2/2$ is the electron energy in the initial ground state, $\boldsymbol{p}$ is its momentum in the final state, and $U_p = F^2/4\omega^2$ is the ponderomotive energy. The sum in Eq. (3) involves contributions from open n-photon channels with $n \geqslant n_0$, where n_0 is the minimum number of photons required to overcome the ponderomotively shifted detachment limit of $U_p - E_0$. The n-photon process amplitude is

$$A_{pn} = \frac{\omega}{2\pi}\int_0^{2\pi/\omega} \Psi_p^*(\boldsymbol{r},t) V_F(t) \Psi_0(\boldsymbol{r},t) d\boldsymbol{r}\, dt. \tag{4}$$

Here

$$\Psi_p(\boldsymbol{r},t) = \exp\left[i(\boldsymbol{p}+\boldsymbol{k}_t)\cdot\boldsymbol{r} - \frac{i}{2}\int_{-\infty}^{t} (\boldsymbol{p}+\boldsymbol{k}_{t'})^2 dt' \right]$$

is the Gordon-Volkov wave function in the length gauge, $\boldsymbol{k}_t = \int_{-\infty}^{t}\boldsymbol{F}(t')dt'$ is the classical electron momentum in the external field. The $-\infty$ in the integrals means that the field is switched on adiabatically.

The wave function $\Psi_0(\boldsymbol{r},t) = e^{-iE_0 t}\Phi_0(\boldsymbol{r})$ of the initial electron state satisfies the Schrödinger equation with the atomic potential $U(\boldsymbol{r})$:

$$\left[\frac{\hat{\boldsymbol{p}}^2}{2} + U(\boldsymbol{r})\right]\Phi_0(\boldsymbol{r}) = E_0\Phi_0(\boldsymbol{r}). \tag{5}$$

In the length gauge (2), only large distances $r \gg 1$ are important for the description of the initial state wave function $\Phi_0(\boldsymbol{r})$. For atomic anions, where the outer electron is bound by polarization forces, the asymptotic form of $\Phi_0(\boldsymbol{r})$ is

$$\Phi_0(\boldsymbol{r}) \underset{r\gg 1}{\sim} \mathcal{A}\frac{e^{-\varkappa r}}{r} Y_{lm}(\hat{\boldsymbol{r}}), \tag{6}$$

where $Y_{lm}(\hat{\boldsymbol{r}})$ is a spherical harmonic function representing the angular part of $\Phi_0(\boldsymbol{r})$. In the zero-range potential approximation for $U(\boldsymbol{r})$, the normalization constant is $\mathcal{A} = \sqrt{\varkappa/2\pi}$, but real negative ions are better described using a corrected value for $\mathcal{A}$ which can be obtained from the asymptotic behavior of the wave function [30].

Besides interaction (2) with the valence electron, the field $\boldsymbol{F}$ also influences the atomic core electrons. Due to the polarizability of the core, $\alpha(\omega)$, the strong laser field induces a dipole moment

$$\boldsymbol{d}(t) = \alpha(\omega)\boldsymbol{F}(t) \tag{7}$$

in the atom. Then, we can account for the core electrons by introducing the field-induced dipole potential $V_d(t)$ in addition to potential (2) of the field interaction with the outer electron. At large distances $V_d(t)$ can be approximated by the point-dipole potential:

$$V_d(t) \underset{r\gg 1}{\sim} \frac{\boldsymbol{d}(t)\cdot\boldsymbol{r}}{r^3} = -\alpha(\omega)\frac{\boldsymbol{r}\cdot\boldsymbol{F}(t)}{r^3}. \tag{8}$$

Let us recall briefly how to account for the potential in Eq. (8) in the case when F does not depend on time. The interaction with a point static dipole does not change the large-r behavior of the radial part of the bound-state wave function [44]. However, the angular part of the latter is strongly affected by the dipole moment. Thus instead of Eq. (6) we have

$$\Phi_0(\boldsymbol{r}) \underset{r\gg 1}{\sim} \mathcal{A}\frac{e^{-\varkappa r}}{r}\mathcal{Z}(\hat{\boldsymbol{r}}), \tag{9}$$

where $\mathcal{Z}(\vartheta,\varphi)$ is a dipole-spherical function. Functions $\mathcal{Z}(\vartheta,\varphi)$ were used in different problems of atomic and molecular physics (see Refs. [39,40] and references therein) and their properties are well known. Below we give a brief summary of results concerning the dipole-spherical functions (for more details see Ref. [45]).

III. ANGULAR FUNCTIONS IN DIPOLE POTENTIAL

The Schrödinger equation for an electron in a static point-dipole potential,

$$V_d^{\text{static}} = -\frac{\boldsymbol{d}\cdot\boldsymbol{r}}{r^3} = -\frac{d\cos\vartheta}{r^2}, \tag{10}$$

can be separated in radial and angular coordinates, and the angular wave functions $\mathcal{Z}_{\ell m}(\vartheta,\varphi)$ satisfy the differential equation

$$-\left[\frac{1}{\sin\vartheta}\frac{\partial}{\partial\vartheta}\left(\sin\vartheta\frac{\partial\mathcal{Z}}{\partial\vartheta}\right) + \frac{1}{\sin^2\vartheta}\frac{\partial^2\mathcal{Z}}{\partial^2\varphi}\right] + 2d\cos\vartheta\mathcal{Z} = \eta\mathcal{Z} \tag{11}$$

and standard boundary conditions consisted in the 2π periodicity in the azimuthal angle φ and the regularity at the polar angles $\vartheta = 0,\ \pi$. The z projection m of the electron orbital momentum is conserved, while the angular momentum l is not conserved due to the l mixing in the nonspherical dipole potential. Its role is played by the eigenvalues $\eta \equiv \eta_{\ell m}(d)$ which can be enumerated by an integer variable ℓ. It is convenient to express $\eta_{\ell m}$ in terms of a noninteger quasimomentum,

$$\tilde{\ell} = -\frac{1}{2} + \sqrt{\eta_{\ell m} + \frac{1}{4}},$$

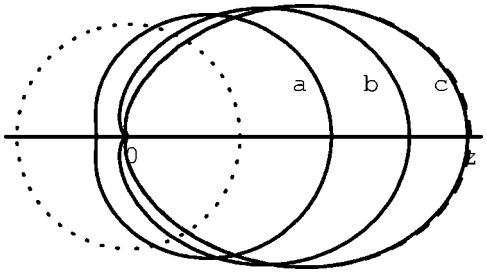

FIG. 1. Polar plot of the absolute value of the dipole-spherical angular functions $\mathcal{Z}_{\tilde{\ell}m}$ for $\ell=m=0$ and the following dipole values: $d=0$ (dotted line), $d=1$ a.u. (a), $d=3$ a.u. (b), $d=6$ a.u. (c). The dashed line corresponds to the complex value $d=(6+2i)$ a.u..

$$\eta_{\ell m} \to \ell(\ell+1), \quad \tilde{\ell} \to \ell \text{ as } d \to 0, \tag{12}$$

which arises instead of the conventional integer angular momentum l. The dipole-spherical angular functions can be decomposed in terms of the familiar spherical harmonics:

$$\mathcal{Z}_{\tilde{\ell}m}(\hat{\mathbf{r}}) = \sum_{l'>|m|} a^m_{\ell l'} Y_{l'm}(\hat{\mathbf{r}}),$$

$$a^m_{\ell l'} \to \delta_{\ell l'} \text{ as } d \to 0, \tag{13}$$

where the coefficients $a^m_{\ell l'} \equiv a^m_{\ell l'}(d)$ satisfy the symmetry conditions

$$a^m_{l l'}(-d) = (-1)^{l+l'} a^m_{l l'}(d) \tag{14}$$

and the recurrence relation

$$2d\left[\frac{l^2-m^2}{4l^2-1}\right]^{1/2} a^m_{\ell l-1} + 2d\left[\frac{(l+1)^2-m^2}{4(l+1)^2-1}\right]^{1/2} a^m_{\ell l+1} = [\eta_{\ell m} - l(l+1)] a^m_{\ell l}. \tag{15}$$

Some more properties of these coefficients are studied in Refs. [39,40].

Figures 1–3 show polar plots of the absolute value of the dipole-spherical angular functions $\mathcal{Z}_{\tilde{\ell}m}$ for various values of d including a complex value. Complex values appear when taking into account the temporal $d(t)$ dependence in the saddle-point approximation, where time t is considered as a complex variable (see next section).

As it is seen from Figs. 1–3, the electron-density distribution is shifted by the dipole towards its positive-charge end, i.e., in the positive direction of the z axis. At the same time,

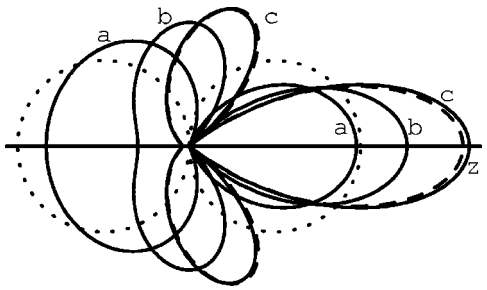

FIG. 2. Polar plot as in Fig. 1 for $\ell=1$, $m=0$.

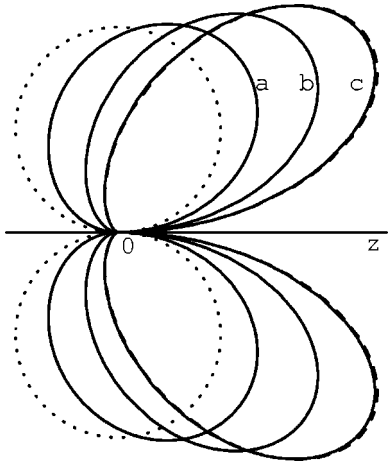

FIG. 3. Polar plot as in Fig. 1 for $\ell=1$, $|m|=1$.

the force due to repulsion from the negative-charge (left) end of the induced dipole acts in the opposite direction. The temporal dependence of the field-induced dipole moment makes the interplay of these factors even more complicated. Mathematically this temporal dependence is accounted for by the effective complex dipole moment which arises in the saddle-point consideration presented in the section below. The analysis of the field-induced dipole effect on strong-field photodetachment requires detailed calculations. Therefore the induced dipole influence on photodetachment can hardly be expressed even qualitatively in a simple and straightforward way.

IV. SADDLE-POINT APPROXIMATION

One should note that the dipole-spherical functions give the exact solution of the angular Schrödinger equation (11) and therefore they provide a nonperturbative account for arbitrary values of the field-induced dipole moment. The only restriction imposed on the field value in a Keldysh-like theory is

$$F \ll F_a \equiv \varkappa^3, \tag{16}$$

where F_a is the internal anionic field.

Another approximation used in Keldysh-like theories is to consider the low-frequency limit

$$\omega \ll |E_0|. \tag{17}$$

In this case the integral in Eq. (4) can be calculated by the saddle-point method [32]. Values of two saddle points $t_{1,2}$ in the complex time plane are determined by

$$\sin \omega t_{1,2} \equiv s_{1,2} = \frac{-\xi \pm i\sqrt{8\zeta(n-\zeta)-\xi^2}}{2\zeta}; \quad s_2 = s_1^*,$$

$$\cos \omega t_{1,2} \equiv c_{1,2} = \pm\sqrt{1-s_{1,2}^2}; \quad c_2 = -c_1^*,$$

$$\zeta = U_p/\omega = \frac{F^2}{4\omega^3}, \quad \xi = \frac{\boldsymbol{F}\cdot\boldsymbol{p}}{\omega^2} = \frac{Fp\cos\theta}{\omega^2}, \tag{18}$$

where θ is the angle between the vectors $\boldsymbol{p}$ and $\boldsymbol{F}$ [not to be mixed up with ϑ in Eq. (11)].

For low frequencies (17) the saddle points (18) are not affected by the induced moment $d(t)$, and the result includes the effective dipole moment value

$$d_{1,2}^{\rm eff}(\omega,F,p,\theta)=\alpha(\omega)F\cos\omega t_{1,2}=\alpha(\omega)Fc_{1,2}(\omega,F,p,\theta),$$

$$d_1^{\rm eff}=-d_2^{\rm eff^*},\quad a_{\ell l'}^m(d_2^{\rm eff})=(-1)^{\ell+l'}a_{\ell l'}^{m^*}(d_1^{\rm eff}).$$

This effective dipole provides an account for the temporal $d(t)$ dependence.

The further calculations are essentially similar to those of Ref. [32]. For the squared amplitude of the n-photon process we obtain

$$\begin{aligned}|A_{pn}|^2=2\pi|M_1|^2\mathcal{A}^2\sum_{l'l''}&|a_{\ell l'}^m(d_1^{\rm eff})a_{\ell l''}^m(d_1^{\rm eff})|\sqrt{(2l'+1)(2l''+1)}\\&\times|P_{l'}^{|m|}(\sqrt{1+p^2\sin^2\theta/\varkappa^2})P_{l''}^{|m|}(\sqrt{1+p^2\sin^2\theta/\varkappa^2})|\\&\times\sqrt{\frac{(l'-|m|)!\,(l''-|m|)!}{(l'+|m|)!\,(l''+|m|)!}}[\cos(\beta_{\ell l'}-\beta_{\ell l''})\\&+(-1)^{\ell+m+n}\cos(\beta_{\ell l'}+\beta_{\ell l''}+\Xi)],\end{aligned}\tag{19}$$

where $P_l^{|m|}$ are Legendre polynomials and

$$M_1=\frac{(c_1+is_1)^n}{\sqrt{-2\pi ic_1(\xi+4\zeta s_1)}}\exp[-ic_1(\xi+\zeta s_1)],$$

$$\Xi=2\arg M_1,\quad \beta_{\ell l'}=\arg a_{\ell l'}^m(d_1^{\rm eff}).\tag{20}$$

For a given value F of the laser field, by integrating Eq. (3) over coordinates ϕ and p of the momentum space we obtain the total differential n-photon detachment probability, i.e., the probability to find the electron emitted at a given angle θ with the momentum value between p and $p+dp$:

$$\frac{dw}{\sin\theta\,d\theta}=\frac{1}{2\pi}\sum_n p|A_{pn}|^2h[p,p+dp;\sqrt{2(E_0+n\omega-U_p)}],\tag{21}$$

where $h(a,b;x)$ is zero anywhere except $a<x<b$; it is expressed in terms of the Heaviside unit step function as $h(a,b;x)=\Theta(x-a)-\Theta(x-b)$.

An important step for comparison of the calculated detachment rate with an experiment consists in averaging over the field spatial and time distributions. The field pulse envelope

$$F^2\equiv F^2(x,y,z,t)=\frac{F_0^2}{1+z^2/z_0^2}\exp\left\{-\frac{(t-z/c)^2}{\tau^2}-\frac{2(x^2+y^2)}{s_0^2(1+z^2/z_0^2)}\right\}\tag{22}$$

is considered to be a focused Gaussian beam of duration τ, focus diameter s_0, and Rayleigh range z_0. Then, the integration over the field distributions can be done analytically [46]. For z_0 large compared with the diameter $\overline{z}$ of the jet of anions, the total number of electrons generated by the pulse is

TABLE I. The saddle-point theory parameters used in calculations for Cs^-.

Peak intensity I_0, W/cm^2	5×10^{11}	1×10^{12}
Field strength F_0, a.u.	0.00377	0.00533
$F_0/F_{\rm internal}=F_0/\varkappa^3$	0.584	0.825
Keldysh parameter $\gamma=\omega\varkappa/F_0$	0.425	0.3
Pondermotive shift $F_0^2/4\omega^2$, a.u.	0.0481	0.0961

$$\begin{aligned}dw^{\rm av}&=\int d^3r\,dt\,dw(F^2(x,y,z,t))\\&=\pi\tau\overline{z}s_0^2\int_0^{F_0^2}dF^2g(F^2)dw(F^2),\end{aligned}\tag{23}$$

where

$$g(I)=\frac{1}{I}\sqrt{\ln\frac{I_0}{I}}h(0,I_0;I),\quad I_0=F_0^2.$$

The integration (23) of Eq. (21) is trivial due to the δ function, and we obtain for the averaged detachment rate

$$\begin{aligned}R(p,\theta)&=\frac{dw^{\rm av}}{\sin\theta\,d\theta}\\&=\frac{\pi\tau\overline{z}s_0^2}{2\pi}\sum_n p\int_0^{F_0^2}dF^2|A_{pn}|^2g[4\omega^2\\&\quad\times(E_0+n\omega-p^2/2)]h\left[p,p+dp;\sqrt{2(E_0+n\omega-U_p)}\right].\end{aligned}\tag{24}$$

Here the binning size dp on the momentum scale is optimized to achieve a continuous shape of the distribution.

V. RESULTS AND DISCUSSION

Calculations of the detachment rate $R(p,\theta)$ were performed for Rb^- and Cs^- anions. These ions have rather close electron affinities: $E_0(Rb^-)=-0.486$ eV, $E_0(Cs^-)=-0.472$ eV. We assumed that the photon energy is $\hbar\omega=0.234$ eV, corresponding to the laser wavelength of approximately 5 μm, and performed calculations for two values of the peak intensity I_0 in the laser focus. These values and relevant parameters of the saddle-point theory are given in Table I. The polarizabilities of neutral atoms $\alpha_{\rm Rb}(\omega)\simeq320$ a.u. and $\alpha_{\rm Cs}(\omega)\simeq400$ a.u. were taken from quantum defect calculations [47].

In order to emphasize the effect we chose comparatively strong-field values, so that the condition (16) is fulfilled less rigorously. In general, when an atomic system is exposed to a very strong electromagnetic field, exceeding the value of the internal field, the details of the electronic structure should play a lesser role in the processes taking place. However, the present work is focused on studying the role of electron correlations under such conditions where the interaction between electrons and the interaction with the laser field are of the same order of magnitude.

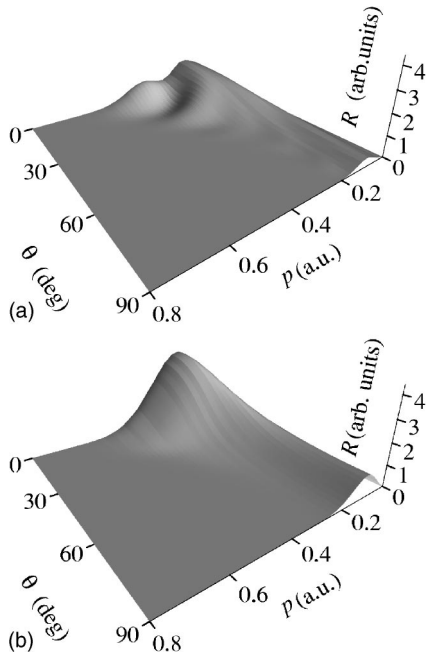

FIG. 4. The momentum-angular distribution $R(p,\theta)$ for Cs^- without account for the core polarization ($\alpha=0$, upper part) and with account for the core polarization ($\alpha=400$, lower part). The peak intensity is $I_0=5\times10^{11}$ W/cm^2.

The results for both anions are essentially similar and therefore we show only predictions for cesium. Photoelectron momentum-angular distributions, $R(p,\theta)$, calculated for the two peak intensities are presented in Figs. 4 and 5, respectively. Sections of these distributions at emission angles θ of 0 and 60° are given in Figs. 6 and 7. The spectra show

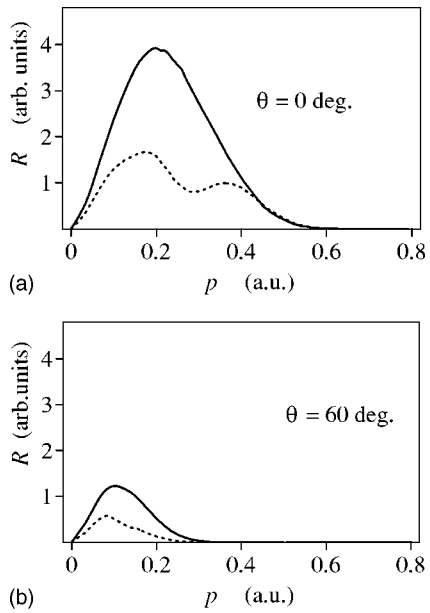

FIG. 5. Photoelectron momentum distribution for Cs^- at emission angles $\theta=0$ (upper part) and 60° (lower part). Solid and dashed lines correspond to calculations with and without account for the core polarization, respectively. The peak intensity is $I_0=5\times10^{11}$ W/cm^2.

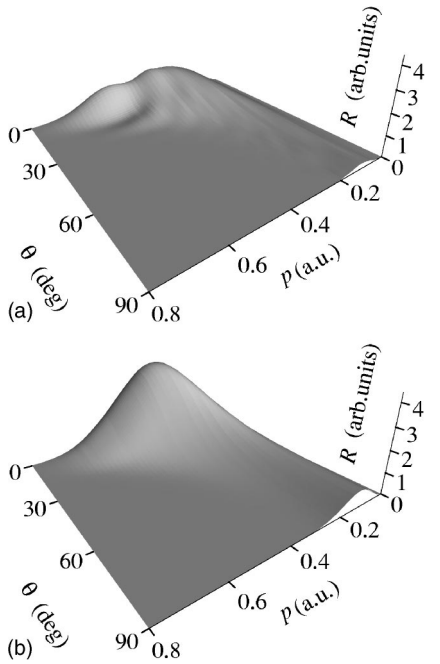

FIG. 6. The same as in Fig. 4, $I_0=1\times10^{12}$ W/cm^2.

contributions from more than 40 excess photon detachment (EPD) channels. The EPD energy peaks are ponderomotively broadened and overlap each other. This results in a rather smooth shape of a spectrum, with the EPD structure hardly resolved.

The spectra calculated without account for the induced dipole effect (see upper parts of Fig. 4 and 5) exhibit a nonmonotonic electron distribution over the momentum coordinate. In particular, these spectra have a local maximum at zero emission angle in the region of higher momenta. Such a maximum is embraced by one or more shoulders at lower momenta. Several EPD peaks are involved to reproduce each fragment of this shape. The nonmonotonic structure is remi-

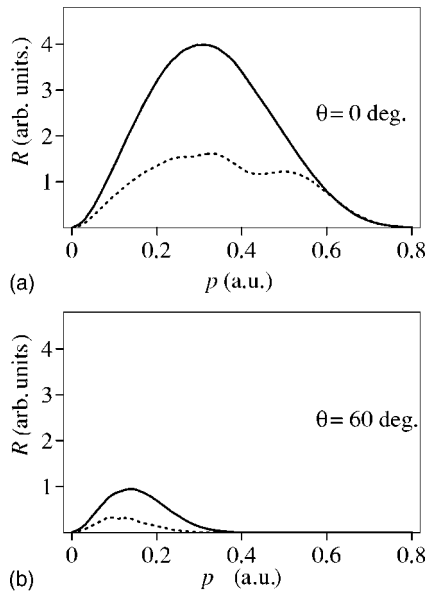

FIG. 7. The same as in Fig. 5, $I_0=1\times10^{12}$ W/cm^2.

niscent of that observed experimentally in the photoelectron spectrum of F^- [6]. It appears due to the quantum interference effect, which we discuss below.

Our results demonstrate a strong modification of the shape of photoelectron spectra due to the action of the field-induced dipole moment in the atomic core. As one can clearly see from Figs. 4 and 5, this effect eliminates the nonmonotonic structure in the shape. In order to understand the origin of such a modification, let us consider closely Eq. (19) describing the transition amplitude. When the induced dipole is absent ($\alpha=0$), the sum over l' and l'' contains only one term with $l'=l''=\ell$. In this case Eq. (19) reproduces the result by Gribakin and Kuchiev [32], where the n-photon transition amplitude to the final state with a given momentum vector $\boldsymbol{p}$ represents a superposition of two saddle-point contributions in the complex time plane. Each saddle point defines an instance on the real time scale, within the oscillation period of the field, at which the electron is released from the core. At these two instances the electron undergoing quiver motion finds itself at opposite sides from the core. This picture simply reflects the fact that in a linearly polarized field the electron can tunnel along either direction of the polarization axis, and it appears as a free electron at a certain distance from the core. Then, the detachment process can be described by two coherent electron emitters, spatially separated and aligned along the laser polarization axis. Their superposition gives rise to interference.

The last term in square brackets in Eq. (19) represents the interference term. When $\alpha=0$, it is reduced to $[1+(-1)^{\ell+m+n}\cos\Xi]$, where Ξ is given in Eq. (20). Here the argument Ξ in cosine describes the phase difference between matter waves propagating in a given direction from the two coherent emitters, respectively. This phase difference depends on the emission angle θ, the electron momentum p, and the laser field parameters F and ω. At fixed values of F, ω, and θ, the interference term oscillates between 0 and 2 as a function of the momentum p. Thus it is the interference effect which causes the nonmonotonic structure in the spectra obtained for $\alpha=0$. The structure modulation is, however, smoothed and does not reach zero. This is because the phase difference is field dependent, and due to the averaging over the intensity distribution in laser focus.

When the field-induced dipole is present, $\alpha\neq 0$, several terms can contribute significantly to the sum in Eq. (19). Each separate term produces an interference structure in the electron spectrum. This structure depends, however, on parameters $\beta_{\ell l'}$ and $\beta_{\ell l''}$, and it appears differently for different terms. As a consequence, the summation over l-mixing terms smears out the interference pattern. It is clear that the number of significant terms in Eq. (19) is determined by the value d of the induced moment. In the Appendix we derive a simple analytical expression for an estimation of l-mixing coefficients. The derivation is performed for the case $\ell=m=0$ relevant to present calculations. One can see from Eq. (A4) that the contribution of l-mixing terms has a Gaussian distribution over l with a width of $d^{1/4}$. It follows that at least four terms ($l'=0$, 1 and $l''=0$, 1) have significant contributions when the value of dipole moment becomes greater than one atomic unit, $|d|\gtrsim 1$. Such a condition is fulfilled in present calculations due to the high polarizability of the Rb and Cs atoms. This condition is sufficient to spoil the interference pattern in a photoelectron spectrum.

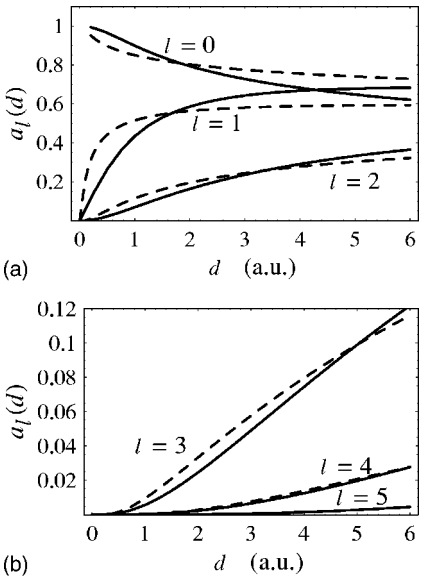

FIG. 8. Dependence of a_{0l}^0 on the dipole moment. Solid lines show numerical results, dashed lines represent the analytical approximation (A4).

Equation (A4) provides a general behavior of l-mixing coefficients. Their values, which are actually used in present calculations, have also been obtained numerically. In Figs. 8 and 9 we compare the analytical and numerical results. Figure 8 shows the approximation (A4) being quite satisfactory for real values of the dipole moment. For its complex values, this approximation is good for $l\lesssim 7$. This can be seen from Fig. 9 where the l dependence of the complex phases $\beta_l=\arg a_l$ is given at $d=(6+2i)$. One can also see that phases β_l have a parabolic dependency on l, as it should be according to Eq. (A4).

We would also like to point out that the account of the field-induced dipole results in an increase of the detachment rate. It means that the above-mentioned repulsion from the negative-charge end of the induced dipole prevails over the charge redistribution. This result, however, is not a general case, rather it depends on the laser field parameters F and ω, the initial state parameters E_0, ℓ, and m, and on the polarizability α of the atomic core. For example, we have performed analogous calculations of a photoelectron spectrum

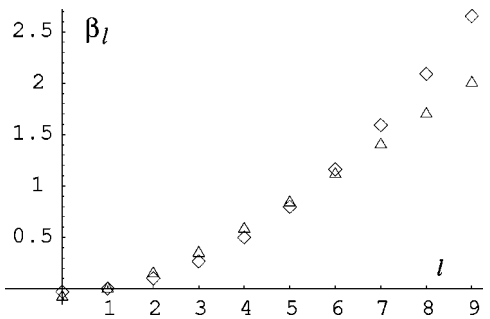

FIG. 9. Dependence of $\beta_l=\arg(a_{0l}^0)$ on l for $d=(6+2i)$: △, numerical results; ◇, analytical approximation (A4).

for Cl^- exposed to a laser pulse of 0.688 eV photon energy and 10^{14} W/cm^2 peak intensity. In this case the dipole effect leads to a decrease of the detachment rate. Because of a small polarizability of the Cl atom, $\alpha_{Cl}=14.7$ a.u., the effect is less prominent, and therefore we do not present this result here.

VI. CONCLUSION

In conclusion, we have presented a simple analytical consideration for the effect of the field-induced atomic dipole moment in the process of photodetachment of negative ions in a strong laser field. The induced dipole is a dynamical many-body effect and it reveals the role of electron correlations in negative ions. We have shown that electron correlations destroy the interference pattern arising in photoelectron spectra in a strong linearly polarized field. The destruction of interference is accomplished due to the strong l mixing representing the angular part of electron correlations. As a result, the shape of the momentum and angular distribution of photoelectrons can be drastically modified under the action of the induced dipole. Such a modification can be resolved experimentally.

The proposed consideration can also be applied in cases where the core polarizability has some peculiarities, such as a resonant enhancement. It may result in even stronger effects of the induced dipole. Such situations are possible in processes involving complex atoms, probably their excited states. The mentioned peculiarities may result even in negative values of the polarizability.

ACKNOWLEDGMENTS

This work was partially supported by the Russian Foundation of Basic Researches (Grant Nos. 02-02-17466 and 04-02-16649) and the Civilian R&D Foundation and Russian MinObrNauka BRHE Program (Grant Nos. VZ-010-0 and Y1-CP-10-04). I.Yu.K. acknowledges support by the Deutsche Forschungsgemeinschaft, Grant No. KI 865/1-1.

APPENDIX: HIGH-l DEPENDENCE OF $a_{\ell l}^m$

Let us consider the behavior of mixing coefficients $a_{\ell l}^m$ in the limit of high angular momenta l and restrict ourselves to the case $\ell=m=0$ relevant to present calculations. Denoting $a_{0l}^0 \equiv a_l$ and $\eta_{00} \equiv \eta$, in this limit the recurrence relation (15) is reduced to

$$(a_{l-1}+a_{l+1})d=(\eta-l^2)a_l, \tag{A1}$$

where $\eta=\sqrt{d}-2d+1/4$. At $l \gg 1$ this difference boundary-value equation can be replaced by the corresponding differential boundary-value equation. The latter can be easily solved in terms of Hermite functions. For $\ell=0$ the solution is reduced to a Gaussian distribution

$$a_l=N(d)\exp\left(-\frac{l^2}{2\sqrt{d}}\right), \tag{A2}$$

where $N(d)$ is defined by the normalization condition

$$\sum_{l=0}^{\infty}|a_l|^2=\frac{1}{2}N(d)^2[1+\vartheta_3(0,e^{-1/\sqrt{d}})]=1, \tag{A3}$$

and ϑ_3 is the elliptic theta function. Since values of the dipole moment involved in present calculations are not very small, we can use an analytical approximation for ϑ_3. As a result we obtain for $d \gtrsim 0.2$ a.u.

$$a_l=\sqrt{\frac{2}{1+\sqrt{\pi}d^{1/4}}}\exp\left(-\frac{l^2}{2\sqrt{d}}\right). \tag{A4}$$

The derivation of Eq. (A4) is not restricted to real values of d and is also valid for its complex values.

[1] C. Blondel, M. Crance, C. Delsart, A. Giraud, and R. Trainham, J. Phys. B **23**, L685 (1990).
[2] H. Stapelfeldt, P. Balling, C. Brink, and H. K. Haugen, Phys. Rev. Lett. **67**, 1731 (1991).
[3] M. D. Davidson, D. W. Schumacher, P. H. Bucksbaum, H. G. Muller, and H. B. van Linden van den Heuvell, Phys. Rev. Lett. **69**, 3459 (1992).
[4] X. M. Zhao, M. S. Gulley, H. C. Bryant, C. E. M. Strauss, D. J. Funk, A. Stintz, D. C. Rislove, G. A. Kyrala, W. B. Ingalls, and W. A. Miller, Phys. Rev. Lett. **78**, 1656 (1997).
[5] R. Reichle, H. Helm, and I. Yu. Kiyan, Phys. Rev. Lett. **87**, 243001 (2001).
[6] I. Yu. Kiyan and H. Helm, Phys. Rev. Lett. **90**, 183001 (2003).
[7] E. J. Robinson and S. Geltman, Phys. Rev. **153**, 4 (1967).
[8] A. W. Weiss, Phys. Rev. **166**, 70 (1968).
[9] D. L. Moores and D. W. Norcross, Phys. Rev. A **10**, 1646 (1974).
[10] M. Cortes and F. Martin, Phys. Rev. A **48**, 1227 (1993).
[11] N. L. Manakov and L. P. Rapoport, Zh. Eksp. Teor. Fiz. **69**, 842 (1975) [Sov. Phys. JETP **42**, 430 (1975)]; I. J. Berson, J. Phys. B **8**, 378 (1975).
[12] M. V. Frolov, N. L. Manakov, E. A. Pronin, and A. F. Starace, Phys. Rev. Lett. **91**, 053003 (2003).
[13] P. A. Golovinskii and B. A. Zon, Opt. Spectrosc. **50**, 569 (1981).
[14] P. A. Golovinskii and B. A. Zon, Izv. Akad. Nauk SSSR, Ser. Fiz. **45**, 12 (1981).
[15] P. A. Golovinskii and B. A. Zon, Opt. Spectrosc. **53**, 125 (1982).
[16] N. B. Delone, I. Yu. Kiyan, V. P. Krainov, and V. I. Tugushev, Opt. Spectrosc. **58**, 157 (1985).
[17] V. K. Ivanov, *Correlations in Clusters and Related Systems. New Perspectives on the Many-Body Problem*, edited by J.-P. Connerade (World Scientific, Singapore, 1996), pp. 73–91.
[18] G. F. Gribakin, V. K. Ivanov, A. V. Korol, and M. Yu. Kuchiev, J. Phys. B **33**, 821 (2000).
[19] H. Bachau, E. Cormier, P. Decleva, J. E. Hansen, and F. Martin, Rep. Prog. Phys. **64**, 1815 (2001).

[20] C. A. Rambsbottom and K. L. Bell, J. Phys. B **28**, 4501 (1995).
[21] M. Dörr, J. Purvis, M. Terao-Dunseath, P. G. Burke, C. J. Jochain, and C. J. Noble, J. Phys. B **28**, 4481 (1995).
[22] N. Miura, T. Noro, and F. Sasaki, J. Phys. B **30**, 5419 (1997).
[23] J. Yuan and L. Fritsche, Phys. Rev. A **55**, 1020 (1997).
[24] N. Vinci, D. H. Glass, H. W. van der Hart, K. T. Taylor, and P. G. Burke, J. Phys. B **36**, 1795 (2003).
[25] H. R. Sadeghpour, C. H. Greene, and M. Cavagnero, Phys. Rev. A **45**, 1587 (1992).
[26] C. Pan, A. F. Starace, and C. H. Greene, J. Phys. B **27**, L137 (1994).
[27] C. N. Liu, Phys. Rev. A **64**, 052715 (2000).
[28] P. A. Golovinskii and I. Yu. Kiyan, Usp. Fiz. Nauk **160**, 97 (1990) [Sov. Phys. Usp. **33**, 453 (1990)].
[29] V. K. Ivanov, J. Phys. B **32**, R67 (1999).
[30] N. L. Manakov, M. V. Frolov, B. Borca, and A. F. Starace, J. Phys. B **36**, R49 (2003).
[31] L. V. Keldysh, Zh. Eksp. Teor. Fiz. **47**, 1945 (1964) [Sov. Phys. JETP **20**, 1307 (1965)].
[32] G. F. Gribakin and M. Yu. Kuchiev, Phys. Rev. A **55**, 3760 (1997).
[33] S. J. Buckman and W. C. Clark, Rev. Mod. Phys. **66**, 539 (1994).
[34] H. W. van der Hart, C. Laughlin, and J. E. Hansen, Phys. Rev. Lett. **71**, 1506 (1993).
[35] I. I. Fabrikant, J. Phys. B **26**, 2533 (1993).
[36] I. B. Bersuker, Opt. Spektrosk. **2**, 97 (1957); S. Hameed, A. Herzenberg, and M. G. James, J. Phys. B **1**, 822 (1968); S. Hameed, Phys. Rev. **179**, 16 (1969); M. G. Veselov and A. V. Shtoff, Opt. Spektrosk. **26**, 321 (1969); I. L. Beigman, L. A. Vainshtein, and V. P. Shevel'ko, *ibid.* **28**, 425 (1970); J. Migdalek and Y.-K. Kim, J. Phys. B **31**, 1947 (1998).
[37] M. Ya. Amusia *et al.*, *Polarization Bremsstrahlung of Particles and Atoms* (Plenum Press, New York, 1993).
[38] V. A. Astapenko, L. A. Bureeva, and V. S. Lisitsa, Usp. Fiz. Nauk **172**, 155 (2002) [Phys. Usp. **45**, 149 (2002)].
[39] B. A. Zon, Zh. Eksp. Teor. Fiz. **102**, 36 (1992) [Sov. Phys. JETP **75**, 19 (1992)].
[40] J. K. G. Watson, Mol. Phys. **81**, 227 (1994).
[41] Th. Mercouris, Y. Komninos, S. Dionissopoulou, and C. A. Nicolaides, Phys. Rev. A **50**, 4109 (1994).
[42] J. Zhang and P. Lambropoulos, J. Phys. B **28**, L101 (1995).
[43] R. Wiehle, B. Witzel, H. Helm, and E. Cormier, Phys. Rev. A **67**, 063405 (2003).
[44] L. D. Landau and E. M. Lifshitz, *Quantum Mechanics. Non-relativistic Theory* (Pergamon, Oxford, 1977).
[45] P. G. Alcheev, V. E. Chernov, and B. A. Zon, J. Mol. Spectrosc. **211**, 71 (2002).
[46] R. Kopold, W. Becker, M. Kleber, and G. Paulus, J. Phys. B **35**, 217 (2002).
[47] V. A. Davydkin, B. A. Zon, N. L. Manakov, and L. P. Rapoport, Zh. Eksp. Teor. Fiz. **60**, 124 (1971).